

Analysis of mutual events of Galilean satellites observed from VBO during 2014-15

R. Vasundhara,^{1*} G. Selvakumar,² and P. Anbazhagan²

¹*Indian Institute of Astrophysics, Bangalore 560034, India*

²*Vainu Bappu Observatory, VBO, Indian Institute of Astrophysics, Kavalur, India*

Accepted XXX. Received YYY; in original form ZZZ

ABSTRACT

Results of analysis of 23 events of the 2014-2015 mutual event series from the Vainu Bappu Observatory are presented. Our intensity distribution model for the eclipsed/occulted satellite is based on the criterion that it simulates a rotational light curve that matches the ground based light curve. Dichotomy in the scattering characteristics of the leading and trailing sides explain the basic shape of the rotational light curves of Europa, Ganymede and Callisto. In case of Io the albedo map from USGS along with global values of scattering parameters work well. Mean values of residuals in ($O - C$) along and perpendicular to the track are found to be -3.3 and -3.4 mas respectively compared to "L2" theory for the seven 2E1/2O1 events. The corresponding R.M.S values are 8.7 and 7.8 mas respectively. For the five 1E3/1O3 events, the along and perpendicular to the track mean residuals are 5.6 and 3.2 mas respectively. The corresponding R.M.S. residuals are 6.8 and 10.5 mas respectively. We compare the results using the chosen model (Model 1) with a uniform but limb darkened disk (Model 2). The residuals with Model 2 of the 2E1/2O1 and 1E3/1O3 events indicate a bias along the satellite track. The extent and direction of bias is consistent with the shift of the light center from the geometric center. Results using Model 1, which intrinsically takes into account the intensity distribution show no such bias.

Key words: methods: observational–techniques: photometric Astrometry and celestial mechanics: astrometry – eclipses – occultations: planets and satellites: dynamical evolution and stability

1 INTRODUCTION

On the basis of the results of the international campaign in 1973 of the mutual events of the Galilean satellites, Aksnes (1976) showed that differences in the observed and predicted mid times and depths of the events can be used to revise the orbital constants of the theory. Subsequent International campaigns and analysis of the observations during the 1979, 1985, 1991, 1997, 2003 and 2009 apparitions have provided an extensive data set of inter satellite astrometric positions (Aksnes et al. 1984; GSO 1991; Vasundhara 1991; Arlot et al. 1992; Mallama 1992; Vasundhara 1994; Arlot et al. 1997; Kaas et al. 1999; Vasundhara 2002; Vasundhara et al. 2003; Arlot et al. 2006, 2009; Emelyanov 2009; Dias-Oliveira 2013; Arlot et al. 2014). Following the success of the jovian mutual events, the technique has been extended to mutual events of

saturnian system in 1995 and 2009 (Thuillot et al. 2001; Mallama et al. 2009; Arlot et al. 2012; Zhang, Liu & Tang 2013), and uranian system in 2007 (Asafin et al. 2009; Christou et al. 2009; Arlot et al. 2013). We report here astrometric results of 23 mutual events of the jovian satellites observed from the Vainu Bappu Observatory (VBO) during 2014-15.

2 OBSERVATIONS AND DATA REDUCTION

The observations were carried out at the 1.3 m J.C.Bhattacharyya telescope which is a F/8 R-C Double Horseshoe telescope by DFM Engineering. The ProEM CCD detector covers a field of $4' \times 4'$ at 0.26 arcsec/pixel resolution. A field of this size enabled registering a comparison satellite in the CCD frame along with the main objects on most occasions. The frames were read at 1 MHz speed in normal mode. The time was read from Telescope control system (GPS time derived through Telescope control soft-

* E-mail: rvas@iiap.res.in(RV), selva@iiap.res.in(GS), anbu@iiap.res.in(PA)

ware by DFM) at the start of data acquisition (UT_{Acqn}) and was put in the FITS header. The exposure start and end instances available from the Lightfield program are accurate up to 1 microsecond. However, due to the delay in accessing UT_{Aqun} from the telescope control system by few tens of microseconds, the UT times are only accurate to 100 μs . The final time scale was converted to UTC at the time of data reduction. Sky conditions were generally poor and only those observations that had a comparison satellite in the CCD frame were found to be useful. Images were obtained before and/or after the event when the satellites were well separated in case of occultation events and eclipse events close to opposition. The derived ratio r given by

$$r = \frac{IS1}{IS1 + IS2} \quad (1)$$

was used to account for the contribution of the occulting or eclipsing satellite if present in the aperture. In Equation 1, IS1 and IS2 are the intensities of the eclipsing/occulting and eclipsed/occulted satellites respectively outside the event. The observed normalized light curve with the contributions from both S1 and S2 is:

$$F(S1, S2, t) = \frac{I(t)}{I(0)}, \quad (2)$$

where $I(t)$ is the combined intensity of S1 and S2 at time "t" during the event and $I(0) = IS1 + IS2$. The observed normalized light curve after removing the contribution of S1 can be written as:

$$f(S2, t) = \frac{I(t) - I(0)r}{I(0) - I(0)r}. \quad (3)$$

Our model computes the intensity variation $f^C(S2, t)$ of S2 during the event. This model light curve could in principle be fitted with $f(S2, t)$ directly. However, we preferred to keep the observed light curve intact and converted instead the computed normalized intensity $f^C(S2, t)$ to $F^C(S1, S2, t)$ using the following relation:

$$F^C(S1, S2, t) = f^C(S2, t)(1 - r) + r. \quad (4)$$

The observed light curve $F(S1, S2, t)$ and the computed light curve $F^C(S1, S2, t)$ were fitted as shown in the next section. Standard R filter was used for all the events. The flux of the objects were extracted using aperture photometry in the APPHOT/DIGIPHOT package in IRAF. Table 1 gives the observing conditions of the twenty three events that were found to be usable for analysis. The integration time was selected between 0.2 - 2 seconds depending on the sky conditions. Column 6 gives the time interval between the data points. The value of 'Q' in column seven is '0' for complete light curves and '1' for light curves for which either immersion or emersion is illdefined. The "ratio" computed using Equation 1 is given in column 8. A value of zero indicates presence of only the eclipsed/occulted satellite in the aperture during flux extraction.

3 MODEL FIT TO THE OBSERVATIONS

3.1 Ephemerides

Ephemerides of Jupiter, the Earth and the Sun were computed using SPICE kernels (Acton 1996) based on DE430.

The positions of the Galilean satellites with respect to Jupiter barycenter were calculated using the theory "L2" by Lainey et al. (2009); the required kernel NOE-5-2010-GAL-a2.bsp available at SPICE was used.

3.2 Selection of albedo and limb darkening model for the satellites

In order to exploit the full potential of the mutual events which are capable of yielding high positional accuracy, it is important to use a realistic intensity distribution on the satellites. The Galilean satellites are known to have rotational light curves implying non uniformity in albedo over their surface (Stebbins 1927; Stebbins & Jacobsen 1928; Morrison & Morrison 1977). Aksnes (1976) pointed out the importance of including surface variations because some light curves were asymmetric giving clear indication that such brightness variations do exist. Vasundhara (2002) used the mosaics of the Galilean satellites constructed by the USGS team and estimated that for central events, the shifts of the photo-center were in the range -50 to $+90$ km (≈ -14 to $+25$ mas) for Io and -30 to $+50$ km (≈ -8 to $+14$ mas) for Europa. Emelyanov & Gilbert (2006) used the albedo maps of the satellites to calculate integrated brightness of the satellites at different rotational phases. They point out that while there are insignificant changes between their modeled and observed rotational light curves by Morrison & Morrison (1977) for Io and Europa, there is deviation for Ganymede. In case of Callisto they find significant discordance. Prokofjeva-Mikhailovskaya and Sergeeva (2012) point out that the spaceborne observations were carried out at a wide range of phase angles while the ground-based observations are limited to $0^\circ - 12^\circ$. They attribute the reason for the discrepancy between groundbased and spaceborne rotational light curves of Ganymede and Callisto to back scattering. It is therefore essential to chose a realistic intensity distribution model. We follow the suggestion by Emelyanov & Gilbert (2006) that the selected distribution should follow the groundbased rotational light curve of the satellites.

Domingue & Verbiscer (1997) derived Hapke's rough surface parameters (Hapke 1984) from disc integrated intensities using Voyager and ground based data for Europa, Ganymede and Callisto. The derived parameters indicate differences in scattering characteristics of the leading and trailing hemispheres. This dichotomy will contribute to the rotational light curve of the satellite. Further, albedo variations due to distributed features are evident in the USGS mosaics; these features will also determine the shape of the rotational light curve. In order to assess the relative contribution of surface dichotomy and albedo variation, we simulated the rotational light curves of the Galilean satellites shown in Figure 1, for a solar phase angle of 6° for the following two scenarios:

(i) Uniform surface but for dichotomy in reflectance properties (DLC: short dashed line): The light curves were constructed by summing the contribution from $1^\circ \times 1^\circ$ elements on the visible surface at orbital longitudes $0^\circ - 360^\circ$. Hapke's parameters by Domingue & Verbiscer (1997) for the leading and trailing sides in the $0.55 \mu m$ wavelength band were used to estimate limb darkening on the satellite disc. For

Table 1. Details of Observations

UT Date yyyy mm dd (1)	Event (2)	Comp. (3)	Seeing arcsec (4)	Airmass (5)	Cycle time sec (6)	Q (7)	Ratio, r (8)
2014 11 27	2O4	J3	2.2	1.142	1.6405	0	0.6624±0.0040
2015 01 26	3E1	J3	2.5	2.333	1.6405	0	0.0000
2015 01 29	1E3	J1	2.2	1.586	1.5405	0	0.0000
2015 01 31	2E1	J4	2.1	1.002	1.3407	0	0.4194±0.0136
2015 01 31	2O1	J4	2.0	1.002	1.3407	0	0.4194±0.0136
2015 01 31	2E4	J1	2.1	1.075	1.4406	0	0.0000
2015 02 12	1E3	J1	3.1	1.309	1.3102	1	0.0000
2015 02 18	2E1	J3	5.0	2.641	3.1408	0	0.4290±0.0059
2015 02 25	2O1	J3	2.4	1.260	1.3407	0	0.4319±0.0024
2015 02 25	2E1	J3	2.1	1.173	1.6405	0	0.0000
2015 02 26	4O2	J3	1.9	1.304	1.4406	0	0.2748±0.0046
2015 03 07	2E4	J3	1.9	1.173	1.6405	0	0.0000
2015 03 11	2O1	J3	1.9	1.259	1.3407	0	0.4396±0.0047
2015 03 11	2E1	J3	2.0	1.725	1.4406	0	0.0000
2015 03 21	2E3	J2	1.8	1.008	4.0220	0	0.0000
2015 03 24	2E4	J2	2.5	1.330	1.7000	0	0.0000
2015 03 28	1E3	J1	1.8	1.015	1.3102	0	0.0000
2015 03 28	2E3	J2	2.2	1.569	1.6100	0	0.0000
2015 04 02	4E3	J4	2.2	1.779	1.6100	0	0.0000
2015 04 04	1O3	J2	1.6	1.005	1.4406	0	0.4211±0.0017
2015 04 05	2E1	J2	2.0	1.079	4.6216	0	0.0000
2015 04 11	1O3	J2	2.4	1.500	1.6100	1	0.4219±0.0029
2015 06 03	3O1	J2	1.8	1.900	1.6405	1	0.5686 ¹

1. From published light curve (Morrison & Morrison 1977) in V magnitude.

Io as only global values of Hapke's parameters reported by McEwen et al. (1988) are available, this simulation could not be carried out.

(ii) Albedo variations inferred by Voyager I & II and Galileo imagery (MLC: long dashed line): No dichotomy in scattering properties on the leading and trailing sides was considered. The albedo maps constructed by various teams were downloaded from the website of United States Geological Survey (USGS)¹. For Io the *NIR* filter mosaic was used to suit our *R* band observations while for the other satellites green filter mosaics were used. Hapke's parameters derived by McEwen et al. (1988) for orange filter were used to estimate the limb darkening for Io. For the other satellites average values of the Hapke's parameters for the leading and trailing sides by Domingue & Verbiscer (1997) were used. The MLC light curves closely resemble the simulations by Emelyanov & Gilbert (2006) in their Figures (1-4), except for some deviation especially for Callisto on the trailing side. This discrepancy may be attributed to the fact that the mosaics used in the two investigations are not the same.

The solid line OLC in Figure 1 is the observed V magnitude rotational light curve from Morrison & Morrison (1977). The light curves in the magnitude scale are shifted to coincide at 0° Central Meridian Longitude (CML) for a better visual comparison, although a critical assessment rests more on the gradient of the light curves. The prime meridian of the

Galilean satellites intersects the equator at the sub-Jovian point. The satellites being in synchronous rotation, the CML follows the orbital longitude and the rotational angle.

A comparison of the groundbased light curve with the simulated light curves shows that:

- (i) For Io, OLC can be closely approximated by MLC.
- (ii) For Europa OLC runs close to both MLC and DLC.
- (iii) There is significant deviation of OLC from MLC as well as DLC for Ganymede especially at eastern and western elongations. Helfenstein & Wilson (1985) derived Hapke's constants for selected regions on Ganymede. The simulated light curves will match closely with the observed rotational light curves if Hapke's constants for more such regions are available and used to estimate limb darkening, instead of using just the albedo map. However as the CML of Ganymede during the 1E3/1O3 and 2E3/2O3 events in 2014-15 were in the range 350°–0°–31° and DLC matches closely with OLC in this region, we selected DLC distribution for Ganymede in our fits to the mutual event data.

(iv) The CML of Callisto when occulted/eclipsed during the present apparition is 345°–360°–21°. In this CML range DLC deviates considerably from OLC indicating significant contribution from distributed bright features. Moor et al. (1999) describe the surface of Callisto to the first order, to be either bright (frost with geometric albedo ≈ 0.8) or dark (geometric albedo ≈ 0.2). As seen in the USGS maps, there are prominent bright regions scattered East of 0° longitude on Callisto. Domingue & Verbiscer (1997) determined Hapke's parameters from disc integrated intensities. It is therefore reasonable to expect that the effect of the bright regions will be to add to the ambient intensity represented by DLC in the 0°-180° region. We therefore consider two basic cases for

¹ Details of the photometric correction processes and mosaic construction are described by Geissler et al. (1999) for Io, Phillips et al. (1997) for Europa, and Becker et al. (1999) for Ganymede and Callisto.

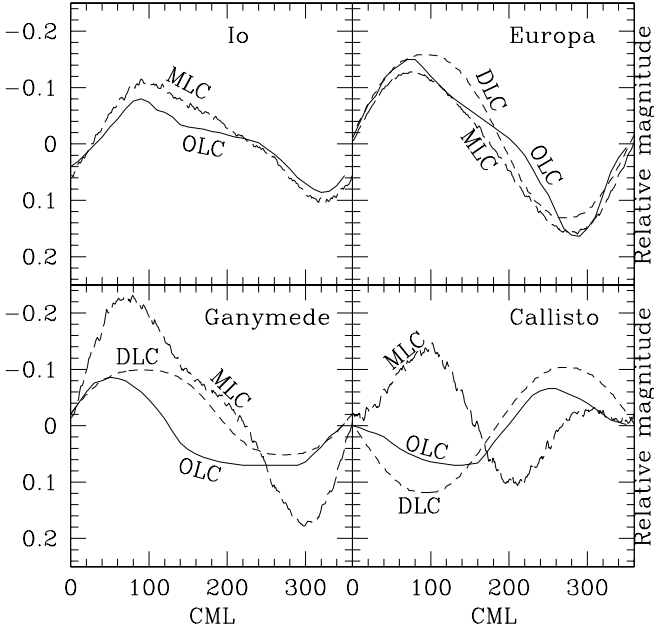


Figure 1. Comparison of rotational light curves. OLC: V magnitude light curve by Morrison & Morrison (1977). DLC: Simulated light curve of the satellite with uniform surface but with dichotomy in reflectance properties on the leading and trailing sides. MLC: Simulated light curve using albedo variations inferred by maps by the USGS and surface without dichotomy (Section 3.2).

Callisto: (1) The DLC model and (2) Convolution of DLC with the mosaic from USGS : DLC^M . The DLC^M model utilizes the Hapke's parameters for the leading and trailing sides to compute the limb darkening (like DLC) but in addition takes into account the albedo map. The same set of Hapke's constants are used for the bright regions. This is a simplistic approach. The center to limb variation in the intensity of the bright frosty regions will not be the same as that of the average terrain due to differences in surface compactness, grain sizes, local slope etc. In absence of information on detailed scattering characteristics of the frosty regions, we adopt the simple scenario mentioned above for DLC^M .

In our chosen model hereafter referred to as "Model 1" we adopt the distributions MLC for Io, DLC for Europa, Ganymede and Callisto. For Callisto we use additionally DLC^M as discussed above.

3.3 Extraction of the parameters

The observed light curves were fitted with theoretical light curves computed using the model presented by Vasundhara (1994). The fit involves comparing the observed (O) and computed (C) light curves using Marquardt's technique. We define the event plane to pass through the geometric center (GC) of the eclipsed/occulted satellite S2. This plane is taken to be perpendicular to the extended heliocentric/topocentric vector to GC of the eclipsed/occulted satellite intersecting the event plane at S1. The two orthogonal parameters that were fitted are :

(i) The correction to the impact parameter " ΔIP ", where IP is the closest distance of the eclipsed/occulted satellite S2 from S1.

(ii) The shift " s " of S2 along the track. A positive value of s indicates that the observed position of S2 is East of its predicted position.

The observed time of close approach of S2 to S1 is obtained from

$$T_{Obs} = T_{Pred} - s/v, \quad (5)$$

where v is the projected relative velocity of S2 with respect to S1 on the event plane. For an easterly motion of S2 with respect to S1 and positive s , the event will be in advance compared to the prediction. The observed IP at the instant T_{Obs} is given by

$$IP = IP_{Pred} + \Delta IP. \quad (6)$$

The separation (X,Y) of S2 from S1 at T_{Obs} along EW and NS on the event plane are calculated from

$$X = IP \times \sin P; \quad Y = IP \times \cos P, \quad (7)$$

where P is the position angle of jovian pole of the date (Archinal et al. 2011). We assume here that the apparent track of S2 relative to S1 is perpendicular to the pole direction of the planet. The derived values of X and Y are independent of the theory. These can therefore be used along with other kind of observations for updating the dynamical constants of the satellites. The residuals (O-C)X and (O-C)Y with respect to L2 ephemerides are given by:

$$(O - C)X = s \times \cos P + \Delta IP \times \sin P \quad (8)$$

$$(O - C)Y = -s \times \sin P + \Delta IP \times \cos P. \quad (9)$$

Tables 2 and 3 give the results of the fits. The first two columns give the UT Date and the event information. The third column gives the intensity distribution that was used in the fit (Section 3.2). Column four gives the fitted observed time T_{Obs} from Equation 5. The derived value of X and Y at the instant T_{Obs} from Equation 7 are given in columns five and six. Columns seven and eight give (O - C) in X and Y from Equations 8 and 9 respectively. The central meridian longitude of the occulted/eclipsed satellite (CML₂) and the solar phase angles are given in the ninth and tenth columns respectively. Column eleven gives the derived impact parameter in arcsec at T_{Obs} . The impact parameter in km is given in column twelve. The fitted light curves and (O-C) residuals of the data points are given in the online version.

The standard deviations of the derived parameters reported in Table 2 and Table 3 are derived from $\sigma \Delta IP$ and σs calculated using the covariance matrix. These estimates therefore depend on the noise which has Poisson distribution, in the data. Other factors such as error in the background subtraction due to proximity of Jupiter or fluctuating sky transparency may produce much larger uncertainty in the derived parameters. The R.M.S. residuals of the mean value of the estimated parameters are determined from the entire data set as shown in the next section. Another source of uncertainty arises because our observations are in R band, due to unavailability of albedo map for Callisto in red filter we used the green filter albedo map. Similarly, use of Hapke's parameters for Europa, Ganymede and Callisto in

Table 2. Results for Occultation events: Fitted observed time, relative inter-satellite distance and ($O - C$) compared to L2

UT Date	Event	Surface model	T_{Obs} (UTC) σT_{Obs} hh mm ss.ss	X arcsec	Y arcsec	(O-C)X σ (O-C)X arcsec	(O-C)Y σ (O-C)Y arcsec	$CML2$ Deg	Phase Deg	IP $\sigma(IP)$ arcsec	Km
(1)	(2)	(3)	(4)	(5)	(6)	(7)	(8)	(9)	(10)	(11)	(12)
2014 11 27	2O4	DLC	22 8 43.81 1.23	0.0764	0.1978	0.0862 0.0051	0.0907 0.0076	18.7	-10.4	0.2120 0.0080	770.2 28.9
2014 11 27	2O4	DLC ^M	22 8 57.88 1.23	0.0400	0.1034	0.0009 0.0066	0.0153 0.0132	18.7	-10.4	0.1109 0.0141	402.9 51.2
2015 01 31	2O1	MLC	19 51 48.73 0.34	-0.1383	-0.3785	-0.0141 0.0015	0.0048 0.0012	282.8	-1.3	-0.4030 0.0012	-1271.9 3.7
2015 02 25	2O1	MLC	15 10 1.16 0.31	-0.0219	-0.0631	-0.0077 0.0025	-0.0183 0.0056	293.2	3.9	-0.0668 0.0059	-213.6 19.0
2015 02 26	4O2	DLC	20 27 57.79 0.76	-0.3066	-0.8837	-0.0348 0.0048	-0.0177 0.0023	340.7	4.1	-0.9354 0.0017	-2996.1 5.6
2015 03 11	2O1	MLC	19 20 44.61 0.28	0.0654	0.1929	-0.0055 0.0017	0.0041 0.0020	298.6	6.5	0.2037 0.0020	667.4 6.7
2015 04 04	1O3	DLC	15 0 44.39 0.81	0.2020	0.6076	-0.0007 0.0034	-0.0093 0.0023	22.1	9.5	0.6403 0.0021	2234.5 7.3
2015 04 11	1O3	DLC	18 0 42.97 2.01	0.2158	0.6491	0.0077 0.0097	-0.0063 0.0062	20.6	10.1	0.6841 0.0056	2438.8 20.1
2015 06 03	3O1	MLC	15 31 31.50 0.75	0.0654	0.1829	0.0047 0.0030	0.0071 0.0046	74.5	9.8	0.1942 0.0048	807.0 19.8

the closest available band at $0.55\mu m$ is cause for some concern.

4 RESULTS AND DISCUSSIONS

Results of the fits using Model 1 for the eight occultation events and fifteen eclipse events are given in Tables 2 and 3 respectively. The time of closest approach of the satellites and the relative astrometric positions at this instant are the actual observed positions, topocentric for occultations and heliocentric for eclipses. These are independent of the theory and can be used along with other sets of observations in construction of future ephemerides.

We consider the two orthogonal parameters ΔIP and s for comparing the observations with predictions instead of the projections (O-C)X and (O-C)Y computed using Equations 8 and 9.

To check the validity of our selection of the limb darkening and albedo model (Model 1) in the present investigation, we fitted the light curves using another scenario (Model 2) in which:

(i) The occulted/eclipsed satellite is uniform, i.e. without albedo variation and also without surface dichotomy.

(ii) The satellite is limb darkened using average value of Hapke's parameters of the leading and trailing sides. For Io the global average values were used.

The derived (O-C) residuals of " s " (along the track) and " ΔIP " (perpendicular to the track) are shown in Figure 2 for Models 1 and 2. Table 4 gives the mean and R.M.S. of the residuals for events of the same type that were observed at least four times. A large number of events are needed for an unequivocal conclusion. However, some trends are evident in Figure 2 and Table 4:

(i) For the 2E1/2O1 events the scatter in (O-C) perpen-

dicular to track in case of Model 2 is significantly larger compared to Model 1, except for the 2E1 event on 18 February observed at large air mass (Table 1). This is also evident from column 5 of Table 4; the R.M.S. values are 7.8 and 19.3 for Models 1 and 2 respectively. Model 1 appears to constrain the estimation of impact parameter better than Model 2. However for the five 1E3/1O3 events which are partial events there are no significant differences either in the mean value or the R.M.S. of the residuals with the two models.

(ii) The mean and R.M.S. residuals along the track for the 2E1/2O1 events with Model 2 are -19.9 and 9.3 mas respectively implying that the fitted times are delayed compared to L2. The delay is marginal for fits with Model 1 which yields mean and R.M.S. residuals of -3.3 and 8.7 mas respectively. Vasundhara (2002) showed that as a result of albedo variation, the light center on Io can shift by ≈ 50 km (≈ 14 mas) towards West when near western elongation. As these events occurred when CMLs were in the range $281^\circ - 313^\circ$, albedo variation may be a likely cause for the delay. Model 2 assumes the disc to be uniform; the deepest part of the light curve is interpreted as the close approach instant of the GC of S2 to S1 thus delaying the fitted time. Model 1 intrinsically takes into account the albedo variation and hence is reliable.

(iii) The mean (O-C) residuals along the track in case of the five 1E3/1O3 events for fits with Models 1 and 2 are 5.6 and 19.3 mas respectively. Model 2 predicts the event to be in advance compared to Model 1; Model 2 detects Ganymede to be east of its actual position. The events occurred within $\pm 25^\circ$ of the superior conjunction of Ganymede. As the leading side is brighter than the trailing side for Ganymede, the light center of its eclipsed/occulted portion will be to the East of the GC of the disc. Model 1 which takes into account this dichotomy has a lower residual while Model 2

Table 3. Results for Eclipse events: Fitted observed time, relative inter-satellite distance and ($O - C$) compared to L2

UT Date	Event	Surface model	$T_{Obs}(UTC)$ σT	X S2-S1	Y	(O-C)X $\sigma(O-C)X$	(O-C)Y $\sigma(O-C)Y$	$CML2$	Phase	IP $\sigma(IP)$	
Date			hh mm ss.ss	arcsec	arcsec	arcsec	arcsec	Deg	Deg	arcsec	Km
(1)	(2)	(3)	(4)	(5)	(6)	(7)	(8)	(9)	(10)	(11)	(12)
2015 01 26	3E1	MLC	15 28 36.86 0.86	0.2802	0.7873	-0.0104 0.0045	0.0107 0.0022	309.6	-2.3	0.8357 0.0017	3230.8 6.4
2015 01 29	1E3	DLC	16 13 36.33 0.79	0.2594	0.7259	0.0088 0.0051	-0.0026 0.0028	350.0	-1.7	0.7708 0.0023	2983.6 9.0
2015 01 31	2E1	MLC	19 36 11.61 0.44	0.1097	0.3062	-0.0059 0.0016	0.0039 0.0012	281.8	-1.3	0.3252 0.0012	1257.4 4.6
2015 01 31	2E4	DLC	21 4 13.84 3.47	-0.3581	-0.9998	-0.0044 0.0150	0.0212 0.0068	345.6	-1.2	-1.0620 0.0045	-4115.0 17.5
2015 01 31	2E4	DLC ^M	21 4 14.47 3.34	-0.3595	-1.0036	-0.0084 0.0144	0.0184 0.0068	345.6	-1.2	-1.0660 0.0048	-4130.7 18.5
2015 02 12	1E3	DLC	21 47 31.50 0.51	0.1353	0.3721	0.0154 0.0031	0.0079 0.0027	344.9	1.3	0.3960 0.0026	1533.8 10.3
2015 02 18	2E1	MLC	13 34 30.27 1.18	0.0515	0.1408	0.0374 0.0057	0.0646 0.0077	291.9	2.5	0.1499 0.0080	580.3 30.9
2015 02 25	2E1	MLC	15 55 4.28 0.10	-0.0107	-0.0290	0.0101 0.0010	-0.0024 0.0025	295.6	3.9	-0.0309 0.0026	-119.6 10.2
2015 03 07	2E4	DLC	14 58 32.26 0.68	-0.1590	-0.4257	0.0497 0.0033	-0.0410 0.0027	12.1	5.7	-0.4544 0.0026	-1764.5 10.0
2015 03 07	2E4	DLC ^M	14 58 38.97 0.71	-0.1420	-0.3803	0.0358 0.0034	0.0159 0.0031	12.1	5.7	-0.4060 0.0030	-1576.3 11.7
2015 03 11	2E1	MLC	20 32 59.37 0.27	-0.0952	-0.2538	0.0027 0.0014	-0.0076 0.0013	302.3	6.5	-0.2711 0.0012	-1050.6 4.8
2015 03 21	2E3	DLC	15 45 59.29 0.87	0.2748	0.7246	0.0084 0.0037	-0.0352 0.0019	30.9	7.9	0.7750 0.0015	3007.8 5.7
2015 03 24	2E4	DLC	18 52 55.72 1.36	-0.2350	-0.6173	0.0534 0.0020	0.0056 0.0011	20.8	8.3	-0.6605 0.0009	-2566.7 3.6
2015 03 24	2E4	DLC ^M	18 53 17.48 1.30	-0.2317	-0.6088	0.0251 0.0019	0.0260 0.0012	20.8	8.3	-0.6514 0.0010	-2531.5 3.7
2015 03 28	1E3	DLC	15 3 36.79 0.29	-0.2122	-0.5555	0.0010 0.0012	0.0162 0.0008	21.1	8.8	-0.5947 0.0007	-2309.2 2.7
2015 03 28	2E3	DLC	19 6 54.20 0.78	0.2045	0.5351	0.0268 0.0035	-0.0352 0.0023	29.5	8.8	0.5729 0.0020	2224.5 7.8
2015 04 02	4E3	DLC	19 13 2.18 12.67	-0.4442	-1.1580	-0.0145 0.0274	0.0372 0.0125	281.3	9.3	-1.2403 0.0073	-4812.7 28.4
2015 04 05	2E1	MLC	16 32 23.36 1.45	-0.2583	-0.6709	-0.0093 0.0084	0.0008 0.0039	312.9	9.6	-0.7189 0.0025	-2790.2 9.5

interprets the light center as the GC and hence the event fitted time is in advance.

(iv) The (O-C) residuals along the track of the two 2E3 events in Figure 2 have large mean residuals of 29 mas and 41 mas for Models 1 and 2 respectively. The data sample being sparse no decisive conclusion can be drawn.

(v) As shown by the arrows connecting DLC to DLC^M positions, the (O-C) residuals of the 2E4/2O4 events improve when the albedo map of Callisto is included. Figure 3 shows the fitted light curves and (O-C) using DLC and DLC^M distributions for the 2O4 event on 27 November 2014. The observed light curve is asymmetric. Distribution DLC (thin solid line) fits only approximately the central portion of the light curve, the (O-C) plot in this region indicates poor fit with a hump indicating unaccounted flux. DLC^M (thick solid line) fits better with smaller (O-C). The relative position of the two satellites at instances 'A', 'B', 'C', 'D' and 'E' marked on the light curve are shown at the top. From the image of Callisto in 'E' it is clear that the eastern segment is dominated by the bright regions: Hepti, im-

pact basin Valhalla, Adlinda, Lofn and Heimdall. Starting from the first contact, the south-eastern bright regions start getting occulted. Between positions 'A' and second contact (position B) the southern part of the segment with bright regions except the southernmost feature Heimdall are occulted. This explains the relatively rapid fall in intensity in this part of the light curve compared to DLC. While DLC distribution yields a light curve that is flat between second and third contacts except for limb darkening effects, DLC^M produces intensity variations in this region. The rise between 'B' and 'C' is due to unveiling of the southern bright group. This is demonstrated in the lower most panel DLC^M - DLC. For annular events the use of albedo map thus appears to improve the fits.

5 CONCLUDING REMARKS

We use our observations of mutual events of the Galilean satellites in 2014-15 from VBO to show that a robust fit

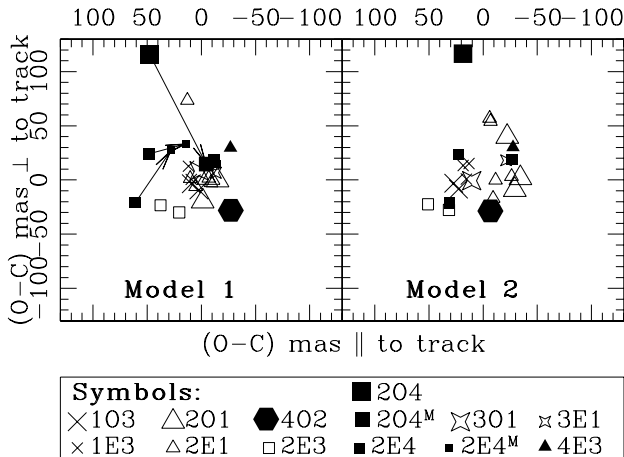


Figure 2. The derived (O-C) residuals along and perpendicular to the track for Models 1 and 2. Model 1 uses the intensity distributions MLC for Io and DLC for Europa, Ganymede and Callisto. For Callisto, DLC^M refers to albedo map + dichotomy in leading and trailing sides. Model 2 uses a uniform disc model without albedo variation except for limb darkening. Symbols for the event pairs are given in the box. $2O4^M$ and $2E4^M$ are fitted positions using DLC^M distribution.

Table 4. Comparison of (O-C) residuals with the two models

Ephm.	Track (O - C)		⊥ to Track (O - C)		Event J1 J2	N
	Mean	R.M.S.	Mean	R.M.S.		
(1)	(2)	(3)	(4)	(5)	(6)	(7)
Model 1	-3.3	8.7	-3.4	7.8	2 1	7
Model 2	-19.9	9.3	10.4	19.3		7
Model 1	5.6	6.8	3.2	10.5	1 3	5
Model 2	19.3	5.7	3.6	10.3		5
Model 1 ¹	5.9	18.9	22.4	9.5	2 4	4
Model 2	11.5	25.4	34.3	34.0		4

1. With DLC^M albedo distribution

to the light curves depends on precise knowledge of intensity distribution on eclipsed/occulted satellites. We set the criterion that a satisfactory distribution must also explain the observed rotational light curve of the satellites. For Io, albedo map by USGS along with global limb darkening constants by McEwen et al. (1988) is found to be satisfactory. Dichotomy in the scattering characteristics of the leading and trailing sides (Domingue & Verbiscer 1997) is able to approximate the observed rotational light curves for the three outer satellites. The departures which are more severe for Ganymede and Callisto can be reduced if Hapke's parameters for prominent terrains on the satellites are available. These parameters will help to estimate the center to limb variation of intensity of the local terrains at different rotational phases.

Our results with uniform disc model (Model 2) indicate bias in the (O-C) residuals along the track for sets of 2E1/2O1 and 1E3/1O3 events in the direction and extent that is consistent with the shift of light center on Io and

Ganymede respectively. No such bias is evident within the R.M.S. limits for results using our chosen intensity distribution model (Model 1). As the events of a given kind occur within a narrow range of orbital longitudes, such a bias will be wrongly interpreted as correction in longitude of either of the satellites. Right choice of a model is therefore important because the theory is already able to make predictions accurate to a few mas (Lainey et al. 2009) and observational techniques have improved enormously.

The time of closest approach of the satellites and the relative astrometric positions at this instant are presented for twenty three events.

ACKNOWLEDGMENTS

We thank the J. C. Bhattacharyya telescope time allocation Committee for liberally allocating time for these observations.

REFERENCES

- Acton C.H. Planetary and Space Science, Vol. 44, No. 1, 65, 1996.
- Aksnes K., Franklin F., 1976, AJ, 81, 464
- Aksnes K., Franklin F., Millis R., Birch P., Blanco C., Catalano S., Piironen J. 1984, AJ, 89, 28
- Archinal B. A. et al., 2011, Celestial Mechanics and Dynamical Astronomy 109, 101
- Arlot J. E. et al., 1992, A&AS, 92, 151
- Arlot J. E. et al. 1997, AAS, 125, 399
- Arlot J.-E. et al. 2006, A&A, 451, 733
- Arlot J.-E., et al., 2009, A&A, 493, 1171A–1182
- Arlot J.-E. et al., 2012, A&A 544, A29.
- Arlot J.-E. et al. 2013, A&A 557, A4
- Arlot, J.-E. et al., 2014, A&A 572 A120
- Assafin, M., Viera-Martins, R., Braga-Ribas, F., Camargo J. I. B., Da Silva Neto D. N., Andrei A. H. , 2009. ApJ, 137, 4046.
- Becker, T. et al. 1999, 30th Annual Lunar and Planetary Science Conf., March 15-29, 1999, Houston, TX, abstract 1692
- Dias-Oliveira, A. et al., 2013, MNRAS, 432, 225
- Christou A. et al. 2009, A&A 497, 589
- Domingue D., Verbiscer, A. 1997, Icarus, 128, 49
- Galilean Satellite Observers (GSO). 1991, AJ, 102, 806
- Geessler P. E., McEwen A. S., Keszthelyi L., Lopes-Gautier R., Granahan J., Simonelli D.P., 1999, Icarus 140, 265
- Emelyanov N. V., 2009, MNRAS 394, 1037
- Emelyanov N. V., Gilbert R., 2006, A&A 453, 1141
- Hapke B. 1984, Icarus 59, 41
- Helfenstein P., Wilson L. 1985, P. Lunar and Planetary Science XVI, 339
- Kaas, A.A., Aksnes, K., Franklin, F., Lieske, J. 1999, Astronomical Journal, 117, 1933
- Lainey, V., Arlot J. E., Karatekin O., Van Hoolst T., 2009, Nat, 459, 957
- Mallama, A., 1992 Icarus 95, 309A–318
- Mallama, A. Mitsuru Sáfma, Pedro V. Sada, Robert J. Modic, Chad K. Ellington 2009, Icarus, 200 265

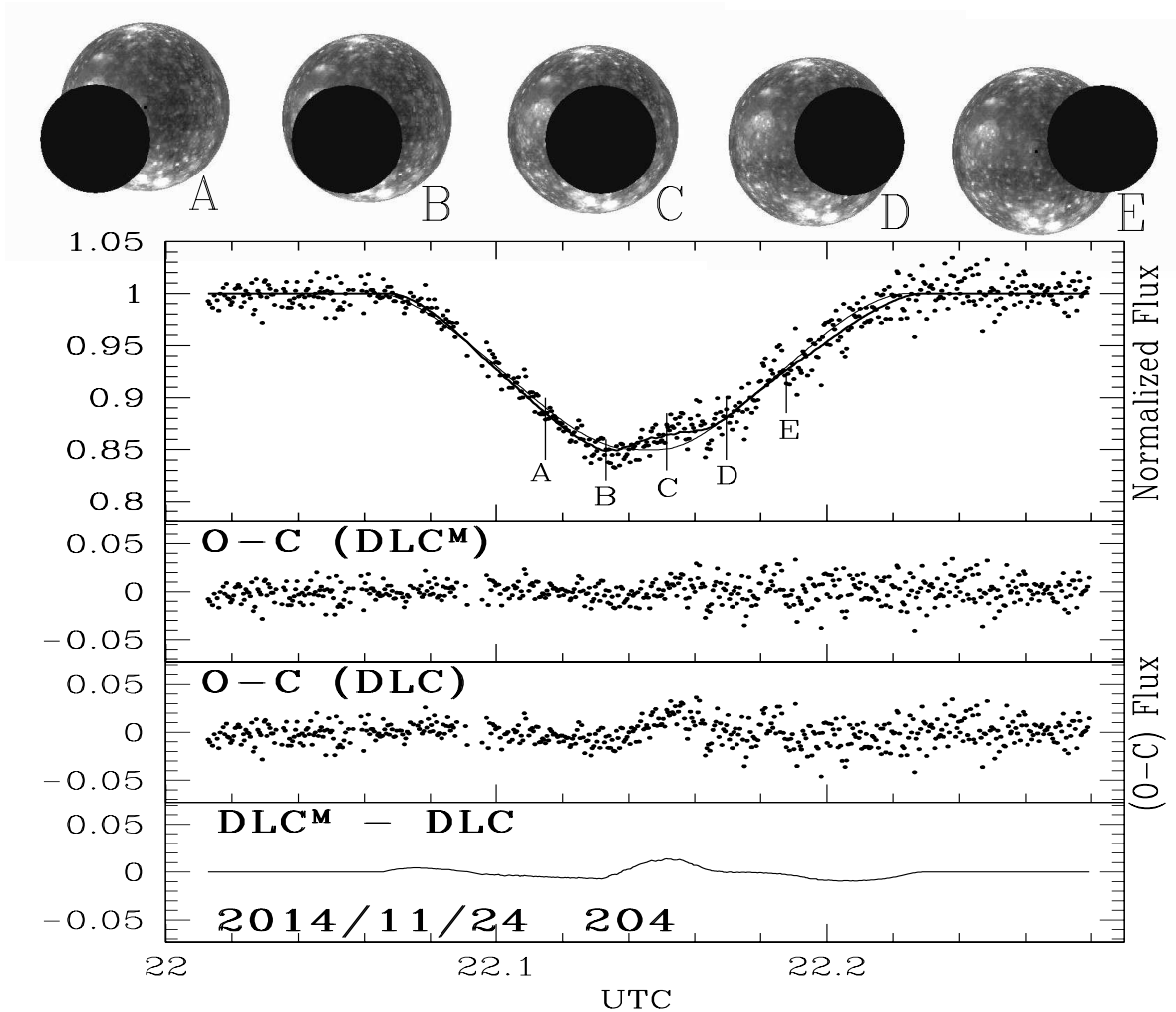


Figure 3. Top panel in the box: Fitted light curves using DLC (Thin solid line) and DLC^M (Thick solid line) of the 204 event on 27 November 2014. The relative positions of the two satellites at instances 'A', 'B', 'C', 'D' and 'E' marked on the light curve are shown above the box. The eastern and South-East segment on the disc of Callisto dominated by the bright regions Valhalla, Adlinda, Lofn and Heimdall is responsible for asymmetry of the observed light curve. The (O-C) residuals for DLC and DLC^M are shown in the two middle panels. The lowermost panel shows the contribution of the segment on the satellite with bright regions in explaining the asymmetry. The O-C is significantly improved in case of DLC^M .

McEwen, A. S., Torrence, V. J., Matson, D. L., & Soderblom, L. A. 1988, *Icarus*, 75, 450
 Moore J. M., et al. 1999, *Icarus* 140, 294–312.
 Morrison D. and Morrison N.D. 1977, in *Planetary satellites* (Tucson: University of Arizona Press), 363–387, *Icarus*, 72, 35
 Phillips C. B., McEwen A. S., Geissler P. E., et al. 1997, *LPSC XXVIII* 103
 Prokofjeva-Mikhailovskaya V. V., Sergeevaa E. A., 2012, *International Journal of Astronomy* 1(3), 49
 Stebbins J., 1927, *Lick Obs. Bull* 13, 1-11
 Stebbins J., T. Jacobsen T., *Obs. Bull.* 13, 180-195, 1928.
 Thuillot W. et al., 2001, *A&A* 371, 343
 Vasundhara R. 1991, *J. Astrophys. Astr.*, 12, 69
 Vasundhara R. 1994, *A&A*, 281, 565

Vasundhara R. 2002, *A&A*, 389 325
 Vasundhara R., Arlot J. E., Lainey V., Thuillot W., 2003, *A&A*, 410, 337
 Xi-liang Zhang, Zhong Liu, Zheng-hong Tang, 2013, *Planetary and Space Science*, 76,83

This paper has been typeset from a \TeX / \LaTeX file prepared by the author.